

Cite this: *Nanoscale Adv.*, 2023, 5, 2493

# Fe<sub>3</sub>O<sub>4</sub>@nano-almond shell@OSi(CH<sub>2</sub>)<sub>3</sub>/DABCO: a novel magnetic nanocatalyst for the synthesis of chromenes†

Mina Keihanfar,<sup>a</sup> Bi Bi Fatemeh Mirjalili <sup>\*a</sup> and Abdolhamid Bamoniri <sup>b</sup>

In this work, we report the synthesis and characterization of Fe<sub>3</sub>O<sub>4</sub>@nano-almond shell@OSi(CH<sub>2</sub>)<sub>3</sub>/DABCO as a novel magnetic natural-based basic nanocatalyst. The characterization of this catalyst was achieved using different spectroscopy and microscopy techniques, such as Fourier-transform infrared spectroscopy, X-ray diffractometry, field-emission scanning electron microscopy, transmission electron microscopy, energy-dispersive X-ray spectroscopy and mapping, vibrating-sample magnetometry, Brunauer–Emmett–Teller measurements, and thermogravimetric analysis. This catalyst was used for the one-pot synthesis of 2-amino-4*H*-benzo[*f*]chromenes-3-carbonitrile from the multicomponent reaction of aldehyde and malononitrile with  $\alpha$ -naphthol or  $\beta$ -naphthol under solvent-free conditions at 90 °C. The yields of the obtained chromenes are 80–98%. The attractive features of this process are its easy work-up, mild reaction conditions, reusability of the catalyst, short reaction times and excellent yields.

Received 18th December 2022  
Accepted 9th March 2023

DOI: 10.1039/d2na00924b

rsc.li/nanoscale-advances

## Introduction

Multicomponent reactions (MCRs) have emerged as the strongest tools in the synthesis of chemotherapeutic drugs, involving the formation of carbon–carbon and carbon–heteroatom bonds using a one-pot procedure.<sup>1–3</sup> In MCRs, a number of different starting components (three or more components) are permissible to react to give a favorable product *via* a one-pot procedure.<sup>4,5</sup> In addition to this, the solvent-free approach is a widely acceptable greener methodology, especially in terms of an economic as well as a synthetic point of view. The use of organic solvents has several disadvantages, including a tiresome work-up procedure, toxicity and high cost.<sup>6–10</sup> Nowadays, nanoparticles are considered to be building blocks for various nanotechnology applications, which mostly display unique size-dependent chemical and physical properties.<sup>11–13</sup> Therefore, derivatization is a prerequisite for any application of nanoparticles, which can be either by activating the surfaces or by stabilizing the functional cores.<sup>14–18</sup>

1,4-Diazabicyclo[2.2.2]octane (DABCO), has been widely used in organic synthesis reactions and can serve as a weak base and ligand. DABCO has received considerable attention as a base catalyst for various organic transformations which is easy to handle, inexpensive, eco-friendly, highly reactive, commercially available, shows efficient activity under neat conditions,

and is non-toxic.<sup>19</sup> Chromene derivatives are potentially important structural units in heterocyclic chemistry that exhibit various omnipresent biological and pharmacological properties, such as cytotoxicity,<sup>20</sup> mutagenicity,<sup>21</sup> antiparasitic<sup>22</sup> and antirhinovirus effects,<sup>23</sup> pesticidal activities<sup>24</sup> and antifungal effects.<sup>25</sup> Additionally, due to their spectroscopic properties they are used for the monitoring of biomolecules and fluorescent compounds in laser technology.<sup>26</sup> Also, chromene derivatives can be effective as a therapy for neurodegenerative diseases, such as Down's syndrome, Parkinson's disease, AIDS-associated dementia, amyotrophic lateral sclerosis, Alzheimer's disease, myoclonus and for the treatment of schizophrenia.<sup>27,28</sup> Many natural compounds including a chromene moiety have been discovered to have anticancer properties. Some of these compounds include calanone (used for leukemia and cervical carcinoma), tephrosin (used for lung cancer), (used for lung, colon, and ovarian cancer), and seselin (used for skin cancer).<sup>29</sup> Thus, the synthesis of highly substituted 4*H*-chromenes and their derivatives has attracted much attention because of their wide applications. Herein, we report an eco-friendly protocol for the synthesis of 2-amino-4*H*-benzo[*f*]chromenes-3-carbonitrile from aldehydes, malononitrile,  $\alpha$ -naphthol or  $\beta$ -naphthol under solvent-free conditions at 90 °C in the presence of Fe<sub>3</sub>O<sub>4</sub>@nano-almond shell@OSi(CH<sub>2</sub>)<sub>3</sub>/DABCO, abbreviated to FNAOSIPD, as a new natural-based green catalyst.

## Experimental

### Materials and methods

Chemicals were purchased from Merck and Aldrich Chemical Companies. <sup>1</sup>H NMR (400, 500 MHz) and <sup>13</sup>C NMR (100 MHz)

<sup>a</sup>Department of Chemistry, College of Science, Yazd University, Yazd, Iran. E-mail: fmirjalili@yazd.ac.ir; Fax: +98 3538210644; Tel: +98 3531232672

<sup>b</sup>Department of Organic Chemistry, Faculty of Chemistry, University of Kashan, Kashan, Iran

† Electronic supplementary information (ESI) available. See DOI: <https://doi.org/10.1039/d2na00924b>



spectra were obtained with a Bruker (DRX-400, Avance). Fourier-transform infrared (FT-IR) spectra were recorded using the attenuated total reflectance (ATR) method on a Bruker (EQUINOX 55) spectrometer. Melting points were found on a Büchi B-540 instrument. The crystallographic characteristics of the sample were obtained using an X-ray diffractometer (XRD, Bruker) using a Cu  $k\alpha$  anode ( $k = 1.54 \text{ \AA}$ , radiation at 40 kV and 40 mA) in the  $2\theta$  range from  $10^\circ$  to  $80^\circ$ . Field emission scanning electron microscopy (FESEM, Mira 3-XMU) and transmission electron microscopy (TEM, CM120) apparatus were used to record of FESEM and TEM images. A vibrating-sample magnetometer (VSM, Meghnatis Daghigh Kavir Co. Kashan Kavir, Iran) was used for measuring the magnetic properties of the catalyst. Energy-dispersive X-ray spectroscopy (EDS) and maps of the catalyst were recorded with a Phenom ProX. Thermogravimetric analysis (TGA) was conducted using a BÄHR-(model: STA 504) instrument. A BELSORP MINI II nitrogen adsorption apparatus (Japan) was used to record the Brunauer–Emmett–Teller (BET) specific surface area of the nanocatalyst at 77 K.

### Synthesis of the catalyst

**Synthesis of nano-almond shell.** Firstly, 5 g of almond shell was well powdered and reacted with 80 ml of 17.5% NaOH solution under reflux conditions for 24 h. Then, the almond shell was filtered and washed with distilled water. It was then bleached with 20 ml of sodium hypochlorite solution and 60 ml of distilled water under reflux conditions for 2 h. Subsequently, the almond shell was filtered and washed well with distilled water. The obtained almond shell powder was added to 80 ml of 35% sulfuric acid aqueous solution and heated under reflux conditions for 6–7 h. The resulting suspension was diluted with water and centrifuged many times to obtain the resulting nano-almond shell.

**Synthesis of  $\text{Fe}_3\text{O}_4$ @nano-almond shell.** 7 g (0.026 mol) of  $\text{FeCl}_3 \cdot 6\text{H}_2\text{O}$  and 2.6 g (0.0130 mol) of  $\text{FeCl}_2 \cdot 4\text{H}_2\text{O}$  were added to a mixture of 2 g of nano-almond shell and 200 ml of 0.05 M acetic acid and mixed for 4 h at  $80^\circ\text{C}$ . Then, 12 ml of 25%  $\text{NH}_4\text{OH}$  was added dropwise into the obtained mixture. After 0.5 h of stirring, using an external magnet, the  $\text{Fe}_3\text{O}_4$ @nano-almond shell was obtained as a black solid (3 g), separated, washed with water, dried at  $80^\circ\text{C}$  and stored.

**Synthesis of  $\text{Fe}_3\text{O}_4$ @nano-almond shell@OSi(CH<sub>2</sub>)<sub>3</sub>Cl.** 1 g of  $\text{Fe}_3\text{O}_4$ @nano-almond shell and 3 ml of 3-chloropropyl trimethoxysilane were dissolved in 10 ml of chloroform. The reaction mixture was heated under reflux conditions for 4 h. Then, the obtained precipitate was separated with an external magnet, washed with dichloromethane and dried at room temperature.

**Synthesis of (FNAOSiPD).** 0.5 g of  $\text{Fe}_3\text{O}_4$ @nano-almond shell@OSi(CH<sub>2</sub>)<sub>3</sub>Cl and (1 mmol, 0.112 g) DABCO were dissolved in 5 ml of dimethylformamide and heated for 24 h at  $80^\circ\text{C}$ . Then the obtained precipitate was filtered, washed with dichloromethane and dried at room temperature.

**Synthesis of 2-amino-4H-chromenes.** A mixture of aldehyde (1.0 mmol),  $\alpha$ - or  $\beta$ -naphthol (1.0 mmol), malononitrile (1.2 mmol) and FNAOSiPD (0.04 g) was stirred at  $90^\circ\text{C}$  under

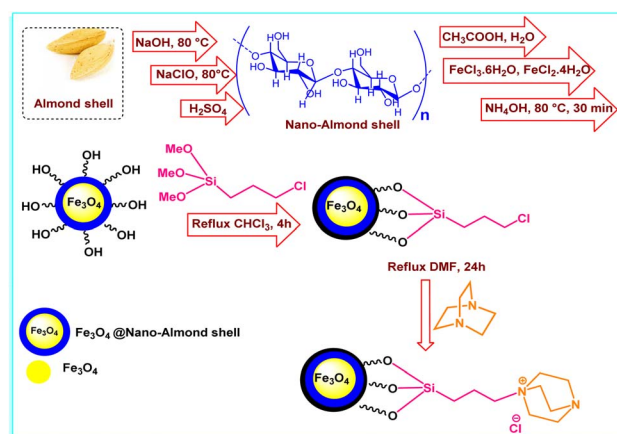
solvent-free conditions. Finally, the obtained mixture was poured into hot ethanol (3 ml) and the catalyst was separated using an external magnet. Then, cold water was added to the residue and the obtained solid product was filtered, washed with water and dried at room temperature.

## Results and discussion

In this research, we have prepared FNAOSiPD *via* a simple procedure that is shown in Scheme 1. Characterization of FNAOSiPD was done with FT-IR, FESEM, TEM, VSM, XRD, BET, EDS, MAPPING and TGA. Then, an efficient and eco-friendly protocol for the synthesis of 2-amino-4H-benzo[*f*]chromenes-3-carbonitrile derivatives in the presence of FNAOSiPD catalyst was introduced.

### FT-IR analysis

The successful functionalization of nano-almond shell can be inferred from a comparison of the FT-IR spectra of the nano-almond shell (Fig. 1, spectrum (a)),  $\text{Fe}_3\text{O}_4$ @nano-almond shell (b),  $\text{Fe}_3\text{O}_4$ @nano-almond shell@OSi(CH<sub>2</sub>)<sub>3</sub>Cl (c), DABCO (d),



Scheme 1 Graphical representation of FNAOSiPD synthesis.

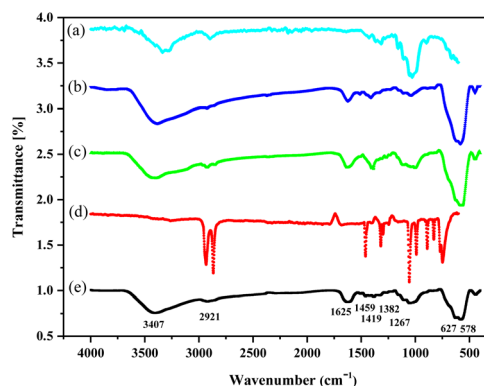


Fig. 1 FT-IR spectra of the (a) nano-almond shell, (b)  $\text{Fe}_3\text{O}_4$ @nano-almond shell, (c)  $\text{Fe}_3\text{O}_4$ @nano-almond shell@OSi(CH<sub>2</sub>)<sub>3</sub>Cl, (d) 1,4-diazabicyclo[2,2,2]octane (DABCO), (e)  $\text{Fe}_3\text{O}_4$ @nano-almond shell@OSi(CH<sub>2</sub>)<sub>3</sub>/DABCO.



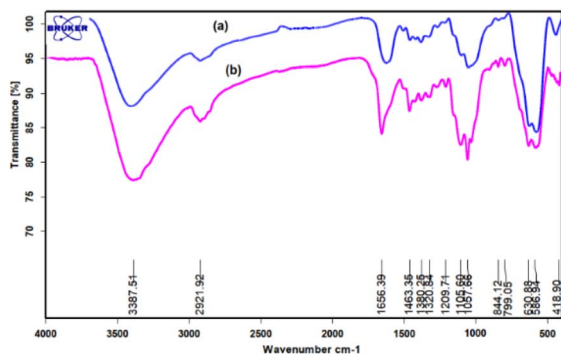


Fig. 2 FT-IR spectra of (a) fresh and (b) reused FNAOSiPD.

FNAOSiPD (e). The bands at  $3400\text{ cm}^{-1}$  in all spectra (a–c and e) and  $2921\text{ cm}^{-1}$  are attributed to O–H and C–H stretching vibration. The band at  $1625\text{ cm}^{-1}$  in all spectra (a–c and e) shows the bending vibration of O–H and the band at  $1455\text{ cm}^{-1}$  shows the  $\text{CH}_2$  bending vibration. The bands at  $1116\text{ cm}^{-1}$  in the (c and e) spectra and at  $1056\text{ cm}^{-1}$  in the (a–c and e) spectra show the stretching vibration of Si–O and C–O bonds, respectively. The broad band near  $600\text{ cm}^{-1}$  in the (b and c, e) spectra shows the Fe/O group.

A comparison between the FT-IR spectra of fresh and reused catalyst shows no changes in any catalyst under the reaction conditions (Fig. 2).

### XRD analysis

Fig. 3 shows the XRD patterns of (a)  $\text{Fe}_3\text{O}_4$  and (b) FNAOSiPD, at  $10\text{--}80^\circ$ . In the XRD spectrum of FNAOSiPD, in addition to the  $\text{Fe}_3\text{O}_4$  signals ( $2\theta = 30^\circ, 35^\circ, 43^\circ, 53^\circ, 57^\circ$  and  $63^\circ$ ), all the detected diffraction peaks ((220) (311) (400) (422) (511) (440)) can be indexed as face centered cubic  $\text{Fe}_3\text{O}_4$  (JCPDS Card No. 19-0629).  $2\theta = 21^\circ$  shows the existence of an  $\text{SiO}_2$  moiety in the structure. A broad peak at  $2\theta = 20\text{--}25^\circ$  is related to the nano-almond shell. The peak position ( $^\circ 2\theta$ ), peak width (FWHM),

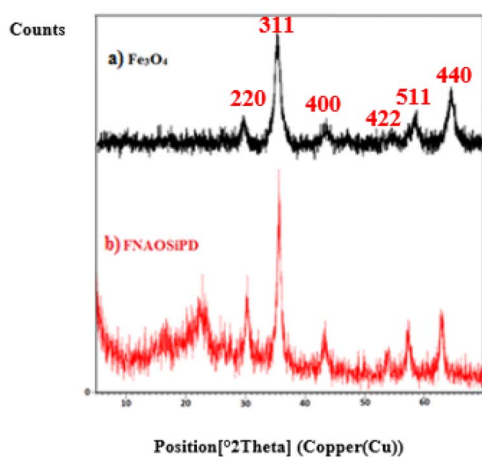


Fig. 3 XRD patterns of (a)  $\text{Fe}_3\text{O}_4$ , (b) FNAOSiPD.

Table 1 The XRD data of FNAOSiPD

| Entry | Peak position [ $^\circ 2\theta$ ] | Peak width (FWHM) | Particle size (nm) |
|-------|------------------------------------|-------------------|--------------------|
| 1     | 22.898                             | 0.787             | 10.4               |
| 2     | 30.204                             | 0.472             | 17.7               |
| 3     | 35.634                             | 0.354             | 24.1               |
| 4     | 43.319                             | 0.63              | 13.7               |
| 5     | 53.737                             | 0.945             | 9.5                |
| 6     | 57.28                              | 0.472             | 19.5               |
| 7     | 62.824                             | 0.787             | 11.9               |

and particle size of the FNAOSiPD were calculated in the range  $22.898$  to  $62.824$ . These results can be found in Table 1. Hence, the particle size (nm) is calculated on the basis of the Debye-Scherrer equation [ $D = K\lambda/(\beta \cos \theta)$ ].

### EDX and EDS-map of FNAOSiPD

The EDX analysis and elemental mapping of FNAOSiPD are shown in Fig. 4 and 5, respectively. EDX analysis and mapping confirm the homogeneous distribution of N, O, C, Fe, Si and Cl in the catalyst with scale bars of  $10\text{ }\mu\text{m}$  (Fig. 5).

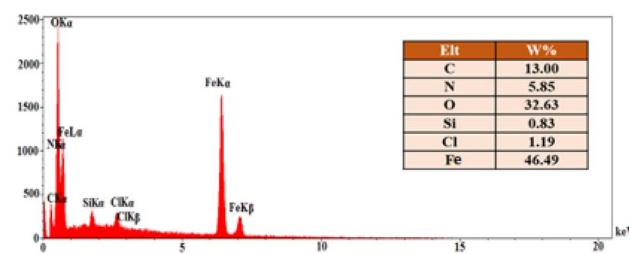


Fig. 4 EDX analysis of FNAOSiPD.

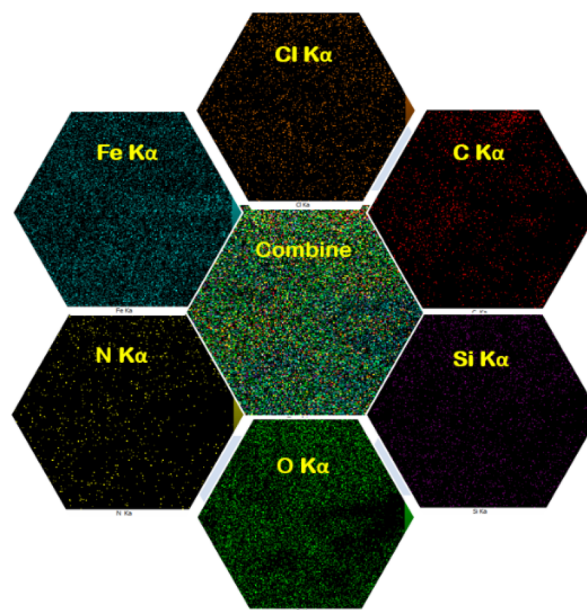


Fig. 5 Elemental mapping images of FNAOSiPD.



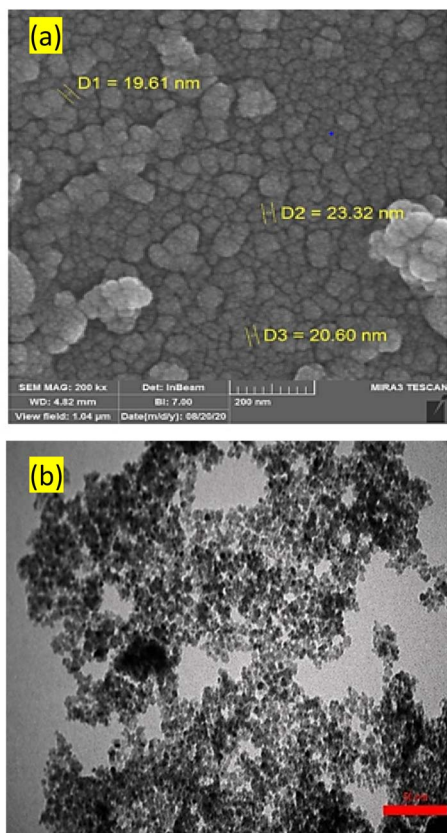


Fig. 6 (a) FESEM and (b) TEM images of FNAOSiPD.

### FESEM and TEM imaging

Fig. 6 presents the results of (a) FESEM and (b) TEM of FNAOSiPD to investigate its particle size and surface morphology. These images indicate that FNAOSiPD nanoparticles have an average size of less than 30 nm.

### Vibrating sample magnetization (VSM) of FNAOSiPD

A vibrating-sample magnetometer (VSM) was used to study the magnetic properties of the catalyst at 300 K by applying a magnetic field ranging from  $-10\,000$  to  $10\,000$  Oe. As shown in (Fig. 7), no hysteresis loop and no remanence were detected

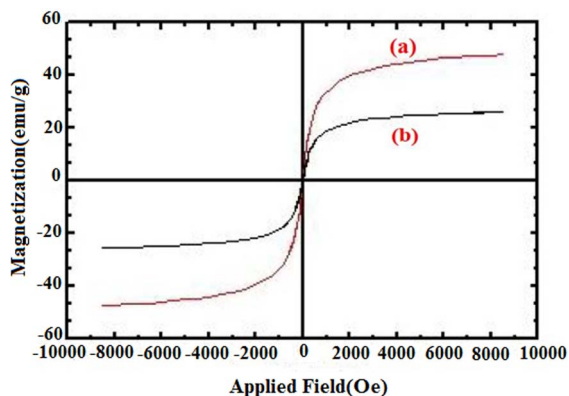


Fig. 7 Magnetization loops of (a)  $\text{Fe}_3\text{O}_4$  and (b) FNAOSiPD.

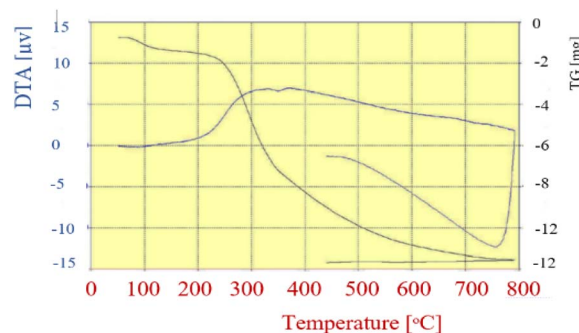


Fig. 8 TGA diagram of FNAOSiPD.

and also the coercivity value was zero for all samples, suggesting a typical superparamagnetic property at room temperature. The saturation magnetization ( $M_s$ ) value for FNAOSiPD is  $25 \text{ emu g}^{-1}$ . This experiment proves the superparamagnetic properties of the catalyst, which can be efficiently separated from the reaction medium with an external magnet.

### TGA-DTA analysis

TG analysis was performed to study the thermal stability of FNAOSiPD from  $50^\circ$  to  $800^\circ$  (Fig. 8). The first endothermic weight loss (less than  $100^\circ\text{C}$ ) is attributed to the removal of catalyst humidity. The weight losses at  $230\text{--}250^\circ$  and  $335^\circ\text{C}$  are attributed to the decomposition of DABCO and almond shell, respectively. The weight reduction from  $387$  to  $800^\circ\text{C}$  is due to the removal and decomposition of  $\text{Fe}_3\text{O}_4$ .

### BET analysis

Fig. 9 shows (a) the adsorption-desorption isotherm of FNAOSiPD, (b) the BJH plot, (c) the t-plot, (d) the BET plot, (e) the

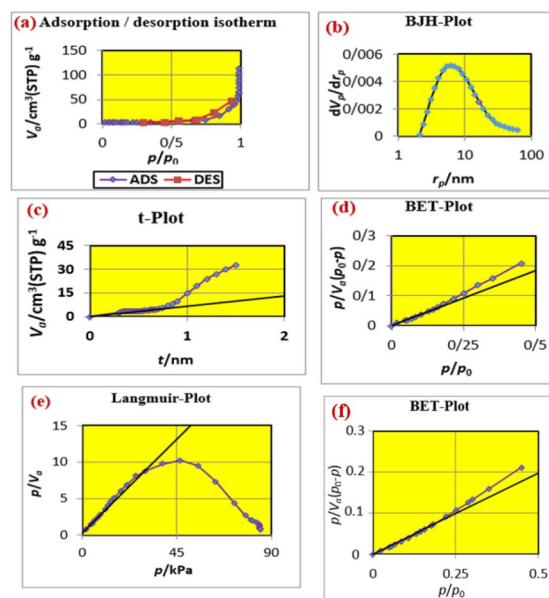


Fig. 9 (a) Adsorption-desorption isotherm, (b) BJH plot, (c) t-plot, (d) BET plot, (e) Langmuir plot of FNAOSiPD and (f) BET plot of reused FNAOSiPD.

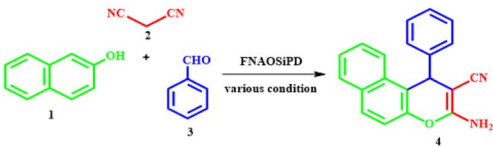


Table 2 Parameters obtained from porosity analysis

| BET plot                              |                   |  |  |
|---------------------------------------|-------------------|--|--|
| $V_m$                                 | 2.7144            | $[\text{cm}^3 (\text{STP}) \text{g}^{-1}]$ |  |
| $a_{s,\text{BET}}$                    | 11.814            | $[\text{m}^2 \text{g}^{-1}]$               |  |
| $C$                                   | 4312.4            |  |  |
| Total pore volume ( $p/p_0 = 0.985$ ) | 0.1749            | $[\text{cm}^3 \text{g}^{-1}]$              |  |
| Mean pore diameter                    | 59.225            | $[\text{nm}]$                              |  |
| Langmuir plot                         |                   |  |  |
| $V_m$                                 | 3.5192            | $[\text{cm}^3 (\text{STP}) \text{g}^{-1}]$ |  |
| $a_{s,\text{lang}}$                   | 15.317            | $[\text{m}^2 \text{g}^{-1}]$               |  |
| $B$                                   | 1.0092            |  |  |
| $t$ -plot                             |                   |  |  |
| Plot data                             | Adsorption branch |  |  |
| $a_1$                                 | 10.036            | $[\text{m}^2 \text{g}^{-1}]$               |  |
| $V_1$                                 | 0                 | $[\text{cm}^3 \text{g}^{-1}]$              |  |
| BJH plot                              |                   |  |  |
| Plot data                             | Adsorption branch |  |  |
| $V_p$                                 | 0.090003          | $[\text{cm}^3 \text{g}^{-1}]$              |  |
| $r_{p,\text{peak}}$ (area)            | 4.61              | $[\text{nm}]$                              |  |
| $a_p$                                 | 13.347            | $[\text{m}^2 \text{g}^{-1}]$               |  |

Langmuir plot and (f) the BET plot of the reused catalyst. The data obtained from the BET, Langmuir,  $t$  and BJH plots are summarized in Table 2.

Table 3 The reaction of benzaldehyde (1 mmol),  $\beta$ -naphthol (1 mmol) and malononitrile (1.2 mmol) in the presence of FNAOSiPD nano-catalyst (0.04 g) under different conditions<sup>a,b,c,d,e</sup>



| Ent. | Solv.            | Cond.  | Catal.                         | Catal. (g) | Time (min) | Yield (%) |
|------|------------------|--------|--------------------------------|------------|------------|-----------|
| 1    | H <sub>2</sub> O | R.T.   | FNAOSiPD                       | 0.04       | 120        | 28        |
| 2    | —                | R.T.   | FNAOSiPD                       | 0.04       | 100        | —         |
| 3    | EtOH             | R.T.   | FNAOSiPD                       | 0.04       | 80         | 60        |
| 4    | H <sub>2</sub> O | Reflux | FNAOSiPD                       | 0.04       | 240        | 70        |
| 5    | —                | 70 °C  | FNAOSiPD                       | 0.04       | 180        | 80        |
| 6    | —                | 80 °C  | FNAOSiPD                       | 0.04       | 240        | 85        |
| 7    | —                | 100 °C | FNAOSiPD                       | 0.04       | 180        | 95        |
| 8    | —                | 110 °C | FNAOSiPD                       | 0.04       | 45         | 88        |
| 9    | —                | 90 °C  | FNAOSiPD                       | 0.03       | 40         | 75        |
| 10   | —                | 90 °C  | FNAOSiPD                       | 0.04       | 50         | 98        |
| 11   | —                | 90 °C  | FNAOSiPD                       | 0.05       | 65         | 90        |
| 12   | —                | 90 °C  | FNAOSiCl                       | 0.04       | 50         | 75        |
| 13   | —                | 90 °C  | FNA/                           | 0.04       | 50         | 65        |
| 14   | —                | 90 °C  | NA                             | 0.04       | 50         | 35        |
| 15   | —                | 90 °C  | Fe <sub>3</sub> O <sub>4</sub> | 0.04       | 50         | 55        |

<sup>a</sup> The molar ratio of aldehyde (mmol), malononitrile (mmol) and  $\beta$ -naphthol (mmol) is equal to 1 : 1.2 : 1. <sup>b</sup> Isolated yields. <sup>c</sup> FNAOSiPD = Fe<sub>3</sub>O<sub>4</sub>@nano-almond shell@OSi(CH<sub>2</sub>)<sub>3</sub>/DABCO. <sup>d</sup> FNAOSi = Fe<sub>3</sub>O<sub>4</sub>@nano-almond shell@OSi(CH<sub>2</sub>)<sub>3</sub>Cl. <sup>e</sup> NA = nano-almond shell.

### Catalyst activity of Fe<sub>3</sub>O<sub>4</sub>@nano-almond shell@OSi(CH<sub>2</sub>)<sub>3</sub>/DABCO

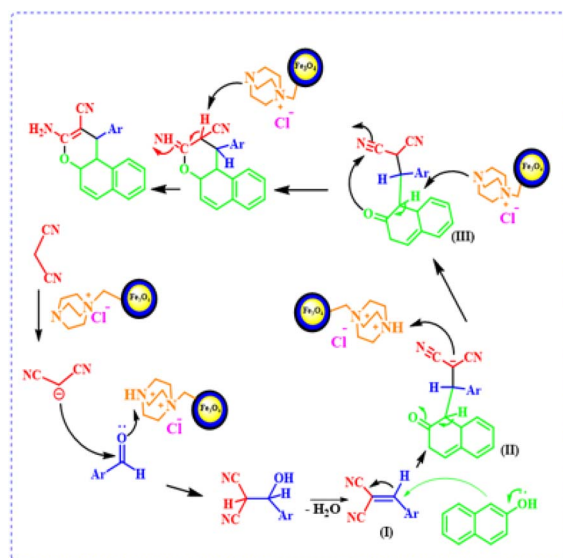
In order to optimize the reaction conditions, the condensation of benzaldehyde (1 mmol),  $\beta$ -naphthol (1 mmol) and malononitrile (1.2 mmol) was chosen as a model reaction. The model reaction was investigated under various conditions, such as the amount of catalyst, solvent, time and temperature (Table 3). The best conditions for the model reaction are solvent-free conditions at 90 °C using 0.04 g of catalyst.

### Proposed mechanism for the synthesis of 4H-chromene derivatives

A plausible mechanism for the synthesis of 4H-chromene derivatives in the presence of the catalyst is shown in Scheme 2. Firstly, the DABCO section in the catalyst acts as a base and converts malononitrile to the corresponding carbanion. The protonated DABCO in the catalyst activates the carbonyl group of the aldehyde. A Knoevenagel condensation reaction between activated aldehyde (1) and malononitrile carbanion (2) leads to the formation of intermediate (I). Then, during a Michael addition reaction,  $\beta$ -naphthol (3) reacts with intermediate (I) as a Michael donor and intermediate (II) is created. Subsequently, the final product is formed by hydrogen transfer and intramolecular cyclization.

According to the above modified conditions, we have synthesized various derivatives of 2-amino-4H-benzo[*f*]chromenes-3-carbonitrile using different aldehydes,  $\beta$ -naphthol or  $\alpha$ -naphthol and malononitrile with good to excellent yields (Table 4). Briefly, aromatic aldehydes bearing both electron-donating and electron-withdrawing groups can successfully produce 2-amino-4H-benzo[*f*]chromenes-3-carbonitrile.

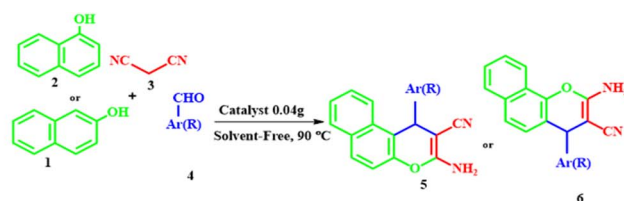
The aromatic aldehydes with electron-donating groups or with steric-hindrance reacted more slowly than aromatic



Scheme 2 Proposed mechanism for the synthesis of 4H-chromene derivatives by using FNAOSiPD.



Table 4 Synthesis of 2-amino-4*H*-benzo[*f*]chromenes-3-carbonitrile derivatives 5a–p, 6a–d using various aldehydes, malononitrile and  $\beta$ -naphthol in the presence of FNAOSiPD



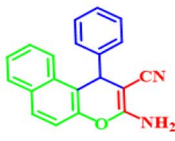
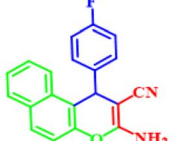
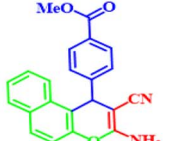
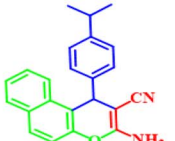
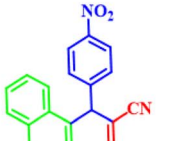

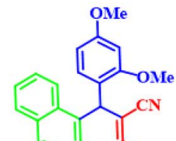

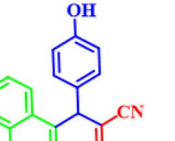
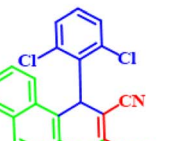
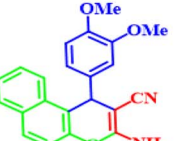
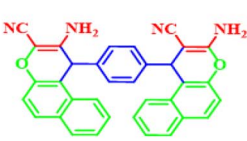




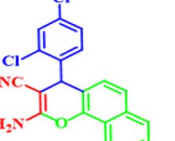

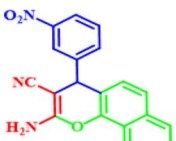

|   |  |  |   |
|---|--|--|---|
| <br><b>5a</b> , Time = 50 min<br>Yield = 98%<br>M. p = 272-274<br>TON (TOF, h <sup>-1</sup> ) = 61.25 (73.79)    | <br><b>5a</b> , Time = 50 min<br>Yield = 98%<br>M. p = 272-274<br>TON (TOF, h <sup>-1</sup> ) = 61.25 (73.79)   | <br><b>5a</b> , Time = 50 min<br>Yield = 98%<br>M. p = 272-274<br>TON (TOF, h <sup>-1</sup> ) = 61.25 (73.79)    | <br><b>5a</b> , Time = 50 min<br>Yield = 98%<br>M. p = 272-274<br>TON (TOF, h <sup>-1</sup> ) = 61.25 (73.79)    |
| <br><b>5b</b> , Time = 60 min<br>Yield = 91%<br>M. p = 185-187<br>TON (TOF, h <sup>-1</sup> ) = 56.87 (56.87)    | <br><b>5f</b> , Time = 120 min<br>Yield = 92%<br>M. p = 220-222<br>TON (TOF, h <sup>-1</sup> ) = 57.5 (28.75)   | <br><b>5j</b> , Time = 95 min<br>Yield = 92%<br>M. p = 151-152<br>TON (TOF, h <sup>-1</sup> ) = 57.5 (36.39)     | <br><b>5n</b> , Time = 65 min<br>Yield = 80%<br>M. p = 210-212<br>TON (TOF, h <sup>-1</sup> ) = 50 (46.16)       |
| <br><b>5c</b> , Time = 100 min<br>Yield = 82%<br>M. p = 282-284<br>TON (TOF, h <sup>-1</sup> ) = 51.25 (32)    | <br><b>5g</b> , Time = 180 min<br>Yield = 94%<br>M. p = 200<br>TON (TOF, h <sup>-1</sup> ) = 58.75 (19.58)    | <br><b>5k</b> , Time = 85 min<br>Yield = 90%<br>M. p = 190-192<br>TON (TOF, h <sup>-1</sup> ) = 56.25 (39.89)  | <br><b>5o</b> , Time = 90 min<br>Yield = 90%<br>M. p = 172-174<br>TON (TOF, h <sup>-1</sup> ) = 56.25 (37.5)   |
| <br><b>5d</b> , Time = 75 min<br>Yield = 93%<br>M. p = 232-233<br>TON (TOF, h <sup>-1</sup> ) = 58.12 (46.49)  | <br><b>5h</b> , Time = 58 min<br>Yield = 95%<br>M. p = 270-271<br>TON (TOF, h <sup>-1</sup> ) = 59.37 (61.84) | <br><b>5l</b> , Time = 185 min<br>Yield = 85%<br>M. p = 255-257<br>TON (TOF, h <sup>-1</sup> ) = 53.12 (17.22) | <br><b>5p</b> , Time = 110 min<br>Yield = 80%<br>M. p = 110-112<br>TON (TOF, h <sup>-1</sup> ) = 50 (27.32)    |
| <br><b>6a</b> , Time = 135 min<br>Yield = 93%<br>M. p = 214-215<br>TON (TOF, h <sup>-1</sup> ) = 58.12 (25.83) | <br><b>6b</b> , Time = 120 min<br>Yield = 96%<br>M. p = 259-260<br>TON (TOF, h <sup>-1</sup> ) = 60           | <br><b>6c</b> , Time = 78 min<br>Yield = 94%<br>M. p = 204-206<br>TON (TOF, h <sup>-1</sup> ) = 58.75 (45.19)  | <br><b>6d</b> , Time = 187 min<br>Yield = 87%<br>M. p = 222-223<br>TON (TOF, h <sup>-1</sup> ) = 54.37 (17.44) |



Table 5 Comparison of FNAOSiPD with other reported catalysts in the model reaction

| Ent. | Catal. (g, mol%, ml)   | Solv.            | Temp. (°C) | Time (min) | Yield (%) | Ref.      |
|------|--|------------------|------------|------------|-----------|-----------|
| 1    | DABCO (30 mol%)  | EtOH             | r.t.       | 360        | 98        | 19        |
| 2    | Mg/Al hydrotalcite (0.072 g)   | S.F.             | 140 MW     | 7          | 84        | 30        |
| 3    | Cetyltrimethylammonium chloride (CTACl) (0.1 ml)                     | H <sub>2</sub> O | Reflux-110 | 360        | 93        | 31        |
| 4    | 1,4-Bis(4-ferrocenylbutyl)piperazine (0.01 g)                        | S.F.             | 100        | 35         | 78        | 32        |
| 5    | 4-Dialkylaminopyridinemagnetic nanoparticles (MNP-DMA 30 mg, 5 mol%) | H <sub>2</sub> O | 80         | 30         | 93        | 33        |
| 6    | 1,8-Diazabicyclo[5.4.0]undec-7-ene (DBU) (10 mol%)                   | H <sub>2</sub> O | 100        | 6          | 94        | 34        |
| 7    | Tetrabutylammoniumbromide (TBABr) (0.8 g)                            | H <sub>2</sub> O | MW         | 2          | 94        | 35        |
| 8    | FNAOSiPD (0.04 g)  | S.F.             | 90         | 50         | 98        | This work |



Fig. 10 Reusability of FNAOSiPD in the synthesis of 5a.

aldehydes with electron-withdrawing groups under the optimized conditions.

According to the EDS data, the amount of N in the catalyst is 5.85%. We have used 0.04 g of catalyst for 1 mmol of substrate (benzaldehyde). Thus, 0.04 g of catalyst contains 0.234 mg of N, equal to  $1.6 \times 10^{-5}$  mol of N. Thus, the TON and TOF of the catalyst are 61.25 and  $73.79 \text{ h}^{-1}$ , respectively.

### Reusability of FNAOSiPD

The reusability of the synthesized magnetic nanocatalyst is one of the most important advantages for industrial use (Table 5). The results confirmed the stability and efficiency of the nanocatalyst for at least 5 times and showed no considerable decrease in catalytic activity (Fig. 10).

## Conclusions

In summary, an organic base DABCO was immobilized on the surface of trimethoxysilane-coated Fe<sub>3</sub>O<sub>4</sub> nanoparticles to afford a functional magnetic catalyst Fe<sub>3</sub>O<sub>4</sub>@nano-almond shell@OSi(CH<sub>2</sub>)<sub>3</sub>/DABCO, which was used in the Knoevenagel reaction of numerous difference aldehydes with malononitrile and naphthols. The results showed that the nanocatalyst MNPs have high catalytic activity, and the reaction products were obtained at nearly quantitative yield within 50–187 min. In

addition to this, the catalyst MNPs can be easily recovered under an external magnetic field, and reused for five runs with almost no loss in activity.

## Data availability

All data generated or analyzed during this study are included in this published article.

## Author contributions

MK, BFM and AB designed and performed the research, analyzed the data, interpreted the results, and prepared the manuscript. MK performed the assay and conducted the optimization, and purification of compounds. All authors read and approved the final manuscript.

## Conflicts of interest

There are no conflicts to declare.

## Acknowledgements

This study was financially supported by Yazd University. The funding bodies played no role in the design of the study and collection, analysis, and interpretation of data and in writing the manuscript. The authors thank the Research Council of Yazd University for supporting this research.

## Notes and references

- 1 A. Dömling, *Chem. Rev.*, 2006, **106**, 17–89.
- 2 Y. L. Gu, *Green Chem.*, 2012, **14**, 2091–2128.
- 3 S. Sajjadifar, S. Rezayati, A. Shahriari and S. Abbaspour, *Appl. Organomet. Chem.*, 2018, **32**, e4172.
- 4 H. G. O. Alvim, E. N. da Silva Junior and B. A. D. Neto, *RSC Adv.*, 2014, **4**, 54282–54299.
- 5 V. G. Santos, M. N. Godoi, T. Regiani, F. H. S. Gama, M. B. Coelho, R. O. M. A. de Souza, M. N. Eberlin and S. Garden, *Chem. Eur. J.*, 2014, **20**, 12808–12816.



- 6 A. Loupy, *Top. Curr. Chem.*, 2008, **206**, 155–204.
- 7 A. F. Mahmoud, F. F. A. El-Latif and A. M. Ahmed, *Chin. J. Chem.*, 2010, **28**, 91–96.
- 8 S. Rezayati, Y. Ahmadi and A. Ramazani, *Inorganica Chim. Acta.*, 2023, **544**, 121203.
- 9 S. Rezayati, F. Kalantari, A. Ramazani, S. Sajjadifar, H. Aghahosseini and A. Rezaei, *Inorg. Chem.*, 2021, **61**, 992–1010.
- 10 M. A. Bodaghifard, Z. Faraki and A. R. Karimi, *Current Org. Chem.*, 2016, **20**, 1648–1654.
- 11 F. Kalantari, S. Rezayati, A. Ramazani, H. Aghahosseini, K. Ślepokura and T. Lis, *ACS Appl. Nano Mater.*, 2022, **5**, 1783–1797.
- 12 H. Liu and A. P. Alivisatos, *Nano Lett.*, 2004, **4**, 2397–2401.
- 13 J. Safaei-Ghomi, R. Teymuri and A. Bakhtiari, *BMC Chem.*, 2019, **13**, 26.
- 14 M. Hamidinasab, M. A. Bodaghifard and A. Mobinikhaledi, *Appl. Organomet. Chem.*, 2020, **34**, e5386.
- 15 M. B. Gawande, A. Goswami, T. Asefa, H. Guo, A. V. Biradar, D.-L. Peng, R. Zboril and R. S. Varma, *Chem. Soc. Rev.*, 2015, **44**, 7540–7590.
- 16 S. Rezayati, A. Ramazani, S. Sajjadifar, H. Aghahosseini and A. Rezaei, *ACS Omega*, 2021, **6**, 25608–25622.
- 17 M. Motahharinia, H. A. Zamani and H. Karimi-Maleh, *Chem. Methodol.*, 2021, **5**, 107–113.
- 18 A. Moghaddam, H. A. Zamani and H. Karimi-Maleh, *Chem. Methodol.*, 2021, **5**, 373–380.
- 19 S. Balalaie, S. Ramezanpour, M. Bararjanian and J. H. Gross, *Synth. Commun.*, 2008, **38**, 1078–1089.
- 20 B. S. Reddy, B. Divya, M. Swain, T. P. Rao, J. S. Yadav and M. V. Vardhan, *Bioorg. Med. Chem. Lett.*, 2012, **22**, 1995–1999.
- 21 K. Hiramoto, A. Nasuhara, K. Michikoshi, T. Kato and K. Kikugawa, *Mutat. Res. Genet. Toxicol. Environ. Mutagen.*, 1997, **395**, 47–56.
- 22 R. Devakaram, D. S. Black, V. Choomuenwai, R. A. Davis and N. K. Umar, *Bioorg. Med. Chem. Lett.*, 2012, **20**, 1527–1534.
- 23 C. Conti, L. Proietti Monaco and N. Desideri, *Bioorg. Med. Chem.*, 2011, **19**, 7357–7364.
- 24 A. M. Shestopalov, Y. M. Emelianova and V. N. Nesterov, *Russ. Chem. Bull.*, 2003, **52**, 1164–1171.
- 25 R. Zhang, Z. Xu, W. Yin, P. Liu and W. Zhang, *Synth. Commun.*, 2014, **44**, 3257–3263.
- 26 C. Sridevi, G. Shanthi and G. Velraj, *Spectrochim. Acta, Part A*, 2012, **89**, 46–54.
- 27 M. F. Dehkordi, G. Dehghan, M. Mahdavi and M. A. H. Feizi, *Spectrochim. Acta, Part A*, 2015, **145**, 353–359.
- 28 H. K. Abd El-Mawgoud, H. A. M. Radwan, F. El-Mariah and A. M. El-Agrody, *Lett. Drug Des. Discov.*, 2018, **15**, 857–865.
- 29 Z. Saffari, H. Aryapour, A. Akbarzadeh, A. Foroumadi, N. Jafari, M. Farahnak Zarabi and A. Farhangi, *Tumor Biol.*, 2014, **35**, 5845–5855.
- 30 M. P. Surpur, S. Kshirsagar and S. D. Samant, *Tetrahedron Lett.*, 2009, **50**, 719–722.
- 31 R. Ballini, G. Bosica, M. L. Conforti, R. Maggi, A. Mazzacani, P. Righi and G. Sartori, *Tetrahedron*, 2001, **57**, 1395–1398.
- 32 M. Hanifeh Ahagh, G. Dehghan, M. Mehdipour, R. Teimuri-Mofrad, E. Payami, N. Sheibani, M. Ghaffari and M. Asadi, *Bioorg. Chem.*, 2019, **93**, 103329.
- 33 S. K. Dangolani, F. Panahi, M. Nourisefat and A. Khalafi-Nezhad, *RSC Adv.*, 2016, **6**, 92316–92324.
- 34 J. M. Khurana, B. Nand and P. Saluja, *Tetrahedron*, 2010, **66**, 5637–5641.
- 35 M. A. Paesha and V. P. Jayashankara, *Indian J. Chem.*, 2007, **46**, 1328–1331.

